Application Note

Cell Analysis

Agilent

Trusted Answers

# Monitoring Drug-Mediated 3D Tumor Spheroid Shrinkage in Real Time Using the Agilent xCELLigence RTCA eSight


**Authors**

Peifang Ye, Grace Yang, and Yunfei Pu
Agilent Biosciences Co. Ltd.
Hangzhou, China

Ryan Raver, Yama Abassi, Nancy Li, and Brandon J. Lamarche
Agilent Technologies, Inc.
San Diego, CA, USA


## Introduction

Because they are expensive, time-consuming, and low-throughput, animal models are typically used for efficacy validation late within the drug discovery and development pipeline. Used at the opposite end of the pipeline, biochemical assays are less expensive and higher throughput, but suffer from the fact that the protein target is analyzed in isolation, removed from the complex cellular milieu within which it has evolved to function. Cell-based assays strike a happy medium between *in vivo* and biochemical assays, enabling protein targets to be evaluated within their endogenous cellular environment while still being relatively inexpensive and high-throughput. However, historically, cell-based assays have been conducted using 2D cell monolayers, and currently there is increasing concern about this format leading to spurious results that are not indicative of clinical efficacy.[1]

Within biological tissues, cells form extensive contacts, on all sides, with other cells and the extracellular matrix. In stark contrast, in tissue culture 2D monolayers, cells form extensive interactions with the rigid glass or plastic surfaces on which they are growing, are exposed to liquid medium on their opposite surface, and interact with neighboring cells only laterally (in the plane of the culture vessel bottom). Within this highly artificial architecture, cells often fail to recapitulate key facets of their *in vivo* phenotype, including morphology, polarity, and drug metabolism.[2] 2D models also fail to challenge cells with the concentration gradients (in oxygen, nutrients, etc.) that they encounter *in vivo*. With that in mind, extensive efforts have been made to develop 3D cell-based assays that are more physiologically relevant. Among these, perhaps the most widely adopted have been spheroids. By culturing cells under conditions that favor cell-cell adhesion above cell-plastic and glass adhesion, cells form aggregates (spheroids) that display physiological hallmarks of solid tumors such as extracellular matrix deposition[3], depth-dependent hypoxia[4], central necrosis[5], and resistance to drug penetration.[6]

Either early during their growth phase, or once they have already grown to substantial size, spheroids can be evaluated for continued growth, stasis, or shrinkage in the presence of different drugs. Although traditional microscopy can be used for assessing drug efficacy, it is tedious, low-throughput, and provides data at very limited temporal resolution. As a significant improvement, this application note demonstrates use of the Agilent xCELLigence RTCA eSight instrument to visually monitor 3D tumor spheroid growth/shrinkage in real time using a combination of brightfield plus red, green, and blue fluorescence. The real time nature of this assay both simplifies the workflow and makes it possible to focus analyses on optimal time windows rather than simply guessing. The Agilent eSight suite of software tools enables drug efficacy ($IC_{50}$) to be calculated based on diverse spheroid metrics such as area, diameter, and brightness.

## Assay principle

eSight is currently the only instrument in the world that interrogates cell health and behavior in real time using a combination of cellular impedance and live cell imaging. Gold biosensors integrated into the bottom of eSight's specialized electronic plates (Agilent E-Plates) continuously monitor changes in cell number, size, attachment strength, and cell-cell adhesion (i.e. barrier function). Within each well of an E-Plate, positioned in between the gold biosensors, a microscopy viewing window enables eSight to capture brightfield and fluorescent (red, green, blue) images from the same population of cells. Using this tandem approach increases the information richness of the assay, providing at least 2x the amount of data without increasing the workload.

While impedance has been used for >20 years to study hundreds of cell lines in diverse assay contexts, including spheroids, this approach is not optimal for spheroids for two specific reasons. First, spheroids cannot be formed directly within eSight's E-Plates; they must first be formed in a different type of plate, then transferred to E-Plate wells, making this approach unsuitable for higher-throughput endeavors. Second, although large in volume, spheroids interact with the E-Plate gold biosensors via a small surface area, resulting in a relatively small impedance signal. For these reasons, eSight was used in this study to monitor spheroids through imaging exclusively. However, when 2D monolayers were assayed, for the purpose of comparing drug efficacy in 2D versus 3D contexts, impedance was used.

Although a variety of techniques have been developed to form spheroids, round-bottom ultralow attachment (ULA) plates are perhaps the most amenable to high-throughput image-based analyses, and were therefore used for the eSight assays described in this study (Figure 1). After seeding cells into a round-bottom ULA plate, a brief centrifugation step helped consolidate the cells in the center of the well. While spheroid aggregation/growth/shrinkage can be monitored by eSight's brightfield images alone, the inclusion of different fluorescent probes is in many cases advantageous. Cell nuclei can be labeled using either the Agilent lentivirus reagents (eLenti) or live cell dyes (eLive).

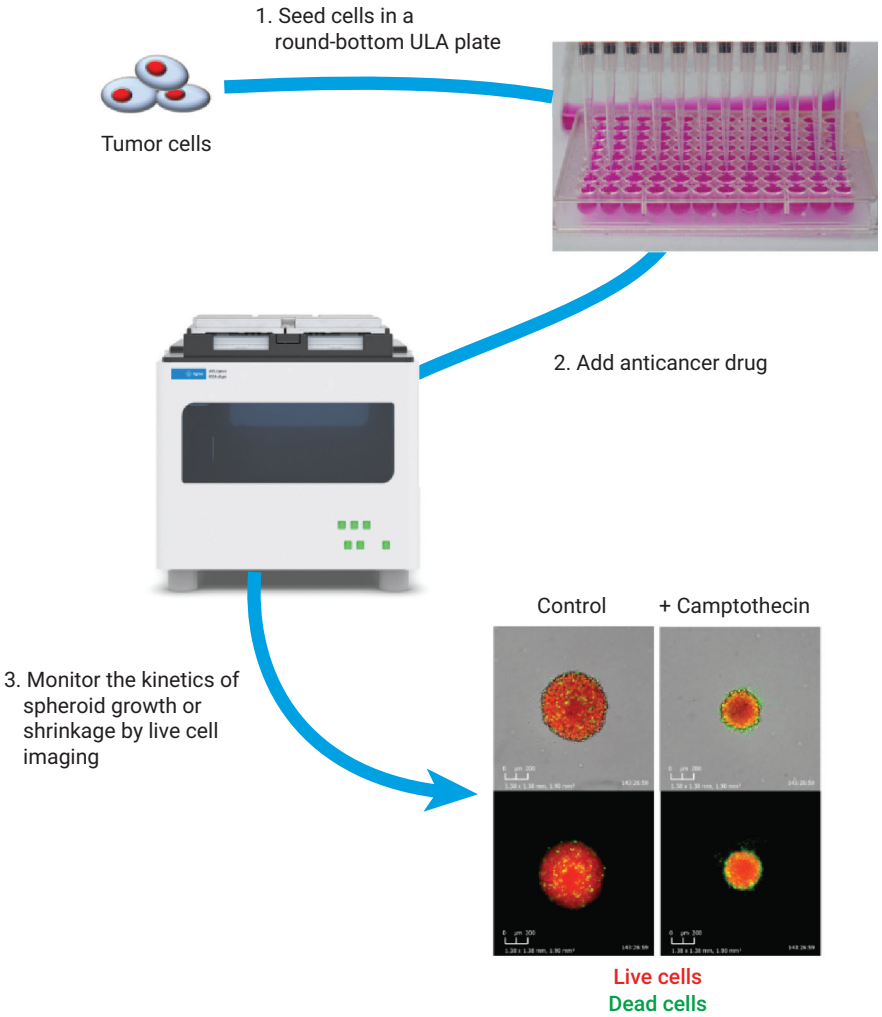


**Figure 1.** Agilent eSight workflow for 3D spheroid assays. See text for details.

Multiplexing is also possible using Agilent eTox dyes to detect dead cells, or Agilent eCaspase and eAnnexin reagents to specifically monitor apoptosis. The eSight software enables the progression of spheroid growth/shrinkage to be quantified readily using parameters such as surface area, diameter, brightness, etc.

## Materials and methods

Cell maintenance and assays were conducted at 37 °C/5% $CO_2$. Cell lines and their growth media are shown in Table 1. FBS was from Gibco (part number 10099-141) and Pen/Strep was from Hyclone (part number SV30010).

HT-1080 Red cells, which express nuclear-localized red fluorescent protein (RFP), were produced by transducing the parental cells with Agilent eLenti Red (part number 8711011). Seventy-two hours after transduction, cells were shifted to complete growth medium containing 2 µg/mL puromycin for an additional 14 days to select for transductants.

For 3D spheroid assays, 150 µL of cell suspension (in complete growth medium) was seeded into each well of a round-bottom ultralow adhesion (ULA) plate (Corning, part number 7007). Plates were subsequently centrifugated at 125 xg for 10 minutes to condense cells in the center of the well. Cell seeding densities varied by cell type; specifics are provided in the Results and discussion section. Plates were then placed into eSight cradles 4 or 5 (which collect images only; impedance is not analyzed in these two cradles), and 3D spheroid growth was monitored continuously. Using the 10x objective, a single photo was collected from each well every 4 hours. Note that if spheroids grow so large that they exceed this single field of view, eSight's 2 × 2 stitching feature can be used to capture a larger area. While brightfield settings were automatically adjusted by the instrument, exposures in the red and green channels were manually set to be 15 to 40 ms (depending on the brightness of the cell line). Three days post cell seeding, the plate was removed from the eSight, and 50 µL of medium containing both anticancer compound and Agilent eTox Green (part number 8711008) was added. Adding both the drug and eTox Green in a single step, and doing so very gently, minimizes any disruption to the spheroid's location/orientation in the well bottom. Spheroid growth or shrinkage was then monitored continuously for an additional 10 days.

**Table 1.** Cell lines and growth media used in this study.

| Cell Lines | Base Medium | Medium Supplements |
|---|---|---|
| HT-1080, MCF7 | EMEM (ATCC, part number 30-2003) | 10% FBS + 1% pen/strep |
| MDA-MB-231, T47D, BxPC3 | RPMI 1640 (Gibco, part number 11875-093) | 10% FBS + 1% pen/strep |
| HeLa, U87 | MEM media (Gibco, part number 11095-080) | 10% FBS + 1% pen/strep |
| A549 | Ham's F-12 (Gibco, part number 11765-054) | 10% FBS + 1% pen/strep |

2D monolayer assays were conducted in Agilent electronic E-Plate VIEW microplates (part number 00300601030) using the same complete growth mediums described previously. After adding 50 µL of media/well, the background impedance was measured. One hundred microliters of cell suspension was then seeded into each well (seeding density = 2,500 cells/well). After allowing cells to settle for 30 minutes at room temperature, the E-Plate was loaded into cradles 1, 2, or 3 of eSight (these cradles collect both impedance and imaging data). While impedance was measured every 15 minutes, images (4 fields of view/well) were collected every 2 hours using the 10x objective. While brightfield settings were automatically adjusted by the instrument, exposures in the red and green channels were manually set to be 60 and 90 ms, respectively. After monitoring cell adhesion and proliferation for ~24 hours, the E-Plate was removed and 50 µL of medium containing both anticancer compound and eTox Green was added to each well. Cytotoxicity was then monitored continuously for an additional 3 days.

## Results and discussion

### Spheroid formation and growth

To interrogate variation in spheroid size as a function of cell seeding density, serial dilutions of HT-1080 Red cells were seeded into round-bottom ULA wells. By simple visual inspection, three days post cell seeding, spheroid size increased in the expected stepwise manner from 313 up through 10,000 cells/well (Figure 2A). Extending out through day 9, the spheroids converged to a common diameter of roughly 750 µm. This plateauing at a common size is especially evident in Figure 2B, where spheroid diameter is plotted as a function of time. Within these plots, note the rapid decrease in spheroid size over the first ~10 hours post cell seeding. Images spanning this short time window demonstrate that this reflects the initially diffuse cells progressively aggregating into a dense cluster (Figure 2C). During this dramatic transition eSight's spheroid-specific segmentation mask (yellow outline) appropriately shifts from recognizing individual cells to recognizing the spheroid as a whole. As an alternative means of tracking spheroid growth, the table in Figure 2D displays percent diameter change as well as rate of growth. These data highlight the fact that seeding a large number of cells immediately produces a large spheroid, but this in turn limits its capacity for growth over an extended time window. This inverse relationship between a spheroid's size and its rate of growth is a consequence of multiple factors, including poor diffusion of nutrients and oxygen into the spheroid's core. These subtleties should be kept in mind when designing assays: spheroid size and growth status over the course of an assay should be tailored to the specific questions one is trying to address.

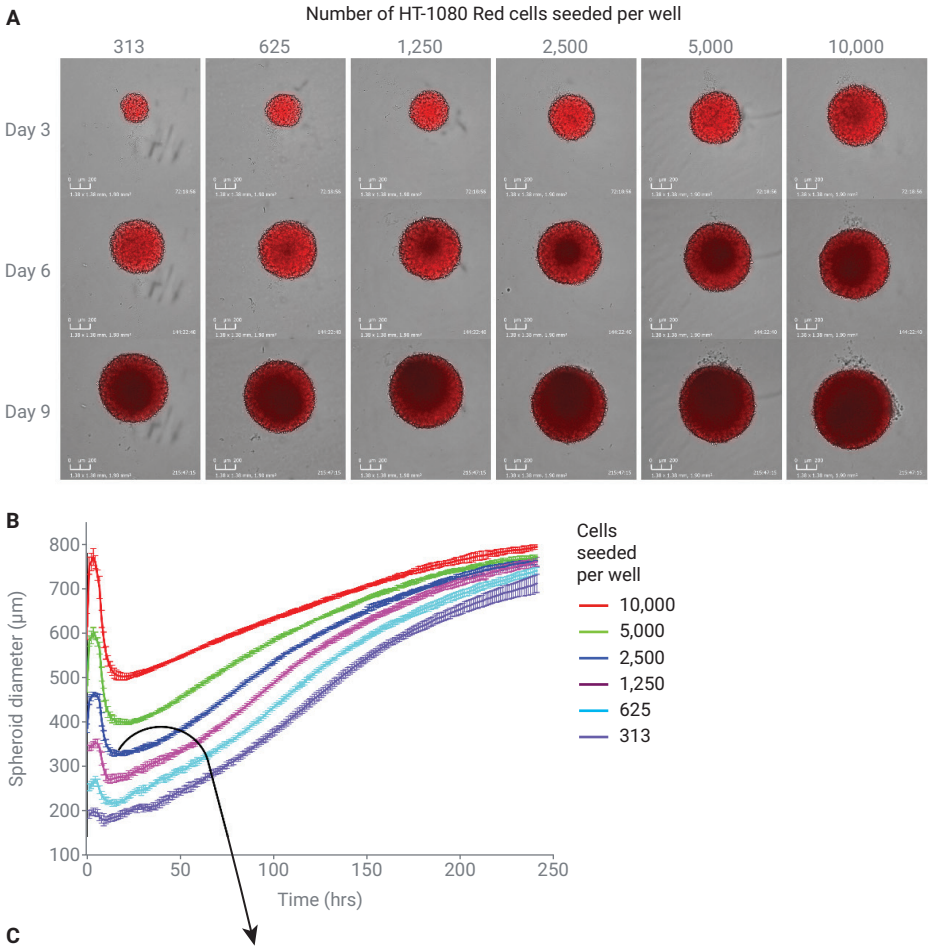


D

| No. of Cells Seeded per Well | Day 1 Diameter (µm) | Day 3 Diameter (µm) | Day 9 Diameter (µm) | % Diameter Change (Day 9 Versus Day 1) | Rate of Diameter Growth (µm/hr) (Day 1 to Day 9) |
|---|---|---|---|---|---|
| 10,000 | 507 ±6 | 589 ±3 | 780 ±9 | 154 ±3% | 1.42 ±0.01 |
| 5,000 | 401 ±5 | 516 ±3 | 759 ±5 | 189 ±3% | 1.86 ±0.02 |
| 2,500 | 334 ±3 | 499 ±3 | 746 ±8 | 223 ±4% | 2.14 ±0.03 |
| 1,250 | 286 ±6 | 394 ±4 | 737 ±8 | 257 ±6% | 2.34 ±0.02 |
| 625 | 239 ±4 | 347 ±4 | 712 ±7 | 298 ±7% | 2.46 ±0.02 |
| 313 | 202 ±5 | 294 ±7 | 681 ±14 | 337 ±7% | 2.49 ±0.02 |

**Figure 2.** Spheroid size and growth rate as a function of cell seeding density. (A) HT-1080 Red cells were seeded at the indicated densities. Although photos were collected by eSight every 4 hours, only representative images taken 3, 6, and 9 days post cell seeding are shown here. Scale bars = 200 µm. (B) Spheroid diameter as a function of time, where diameter was automatically calculated by the eSight software based on red surface area and the equation: $\text{Diameter} = 2 \times \sqrt{\frac{\text{Area}}{\pi}}$ (C) Time course of images from a single well seeded with 2,500 cells, highlighting the rapid condensation/clustering of cells that is responsible for the curve shapes observed over the 0 to 10 hour time window in panel B. (D) Alternative means of tracking spheroid status using % diameter change and rate of diameter growth.

Not surprisingly, the characteristics of spheroids vary depending on the cell line from which they are assembled. Figure 3 shows spheroids 72 hours after seeding 2,500 cells/well. Whereas HeLa, HT-1080, and U87 cells give rise to highly regular spheres, T47D and MCF-7 spheroids are more ovoid, and BxPC3, MDA-MB-231, and A549 spheroids display a high degree of surface irregularity. Also note that within the size range examined, each cell line gives rise to spheroids with differing density/opacity. Despite this broad range of physical characteristics, the eSight software still accurately demarcates each spheroid's boundaries (cyan segmentation masks in Figure 3). Importantly, this holds true both when using brightfield alone (Figure 3) and when using fluorescent images (Figure 2C).

## Anticancer compound mediated spheroid shrinkage

To assess eSight's ability to characterize the efficacy of anticancer compounds against spheroids, HT-1080 Red cells were seeded in a round-bottom HLA plate at a density of 2,500 cells/well. Seventy-two hours after seeding, camptothecin was added at varying concentrations along with Agilent eTox Green dye – which stains dead cells fluorescent green*. Images were acquired for 10 days following drug addition. Starting with the brightfield images in Figure 4A to establish a frame of reference, it is clear that spheroids exposed to the negative control (DMSO) grow progressively larger over time. In contrast, 12.4 nM camptothecin is able to suppress spheroid growth and 1 µM camptothecin actually causes spheroid shrinkage. It is important to note that under some conditions the extent of cell death can be difficult to quantify accurately when using brightfield images alone. For example, on day six the spheroid treated with 12.4 nM camptothecin is comprised of a dense and opaque core that is surrounded by peripheral layers of a more transparent material (the outer boundary of which is denoted by the cyan segmentation mask in this particular photo only). Whether this peripheral material is comprised of living versus dead cells, apoptotic bodies, cell debris, etc. is not clear from the brightfield image alone. When this same spheroid is imaged using red fluorescence alone (Figure 4B), only the dense core retains the RFP signal, while the peripheral material is colorless. This is highlighted in Figure 4C where the brightfield image (denoted by a single asterisk) is superimposed with the red fluorescent image (denoted by double asterisks). This loss of red fluorescence in the spheroid's periphery is consistent with RFP having been degraded through apoptosis, suggesting that this region does not contain living cells. An important implication of the above data is that the red fluorescent images derived from nuclear RFP expression provide an accurate assessment of viable cells in the spheroid, while brightfield images have the potential to overestimate the number of viable cells. This hazard can be minimized through careful adjustment of the brightfield segmentation mask.

* For healthy cells eTox Green is membrane impermeable. As cells undergo apoptosis and their plasma membrane is disrupted, eTox Green gains access to and binds to dsDNA – whereupon its fluorescence increases dramatically.

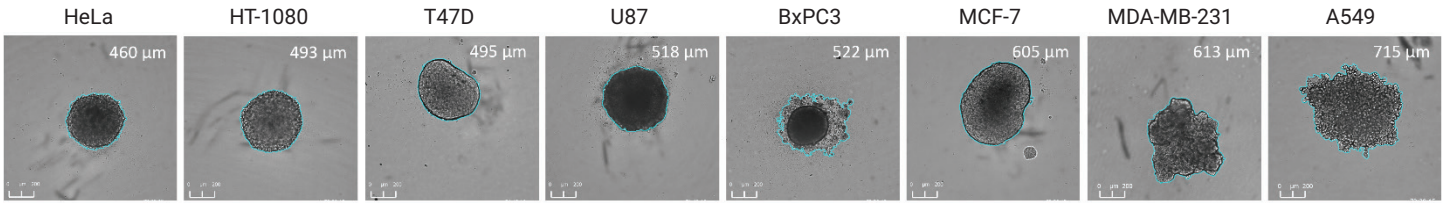


**Figure 3.** Spheroid size, shape, and density/opacity varies for each cell line. 2,500 cells were seeded per well, and images were collected 72 hours later. The cyan line is the Agilent eSight's segmentation mask, demarcating the boundary of each spheroid. Spheroid diameters are listed in white text. Scale bars = 200 µm.

The green fluorescent signal in Figure 4D highlights which regions of the spheroids contain dead cells. To help locate these dead cell regions within the spheroid as a whole, Figure 4E superimposes them with the red fluorescent signal derived from nuclear RFP expression. Visual inspection of the green dead cell images reveals the coexistence of two opposing processes. In the absence of drug the area and intensity of the green dead cell signal continues to increase over time (Figure 4D). In contrast, in the presence of 1 µM camptothecin, the area and intensity of the green dead cell signal decreases over time due to cell lysis (perhaps the result of secondary necrosis). In this scenario, where the fluorescent signal changes in opposite directions depending on drug concentration, assiduous data analysis is especially important (see below). Another important finding relates, again, to the 12.4 nM camptothecin sample from day 6. When the brightfield image is superimposed with the eTox Green image in Figure 4F the brightfield segmentation mask clearly encompasses peripheral regions that contain only a small number of green dead cells. To summarize, combining the brightfield images with the red and green fluorescent images indicates that under some conditions peripheral regions of a spheroid can contain material that: i) does not include living cells (RFP signal is lost), and ii) is only partially comprised of dead cells (based on minimal staining by eTox Green, which is a traditional

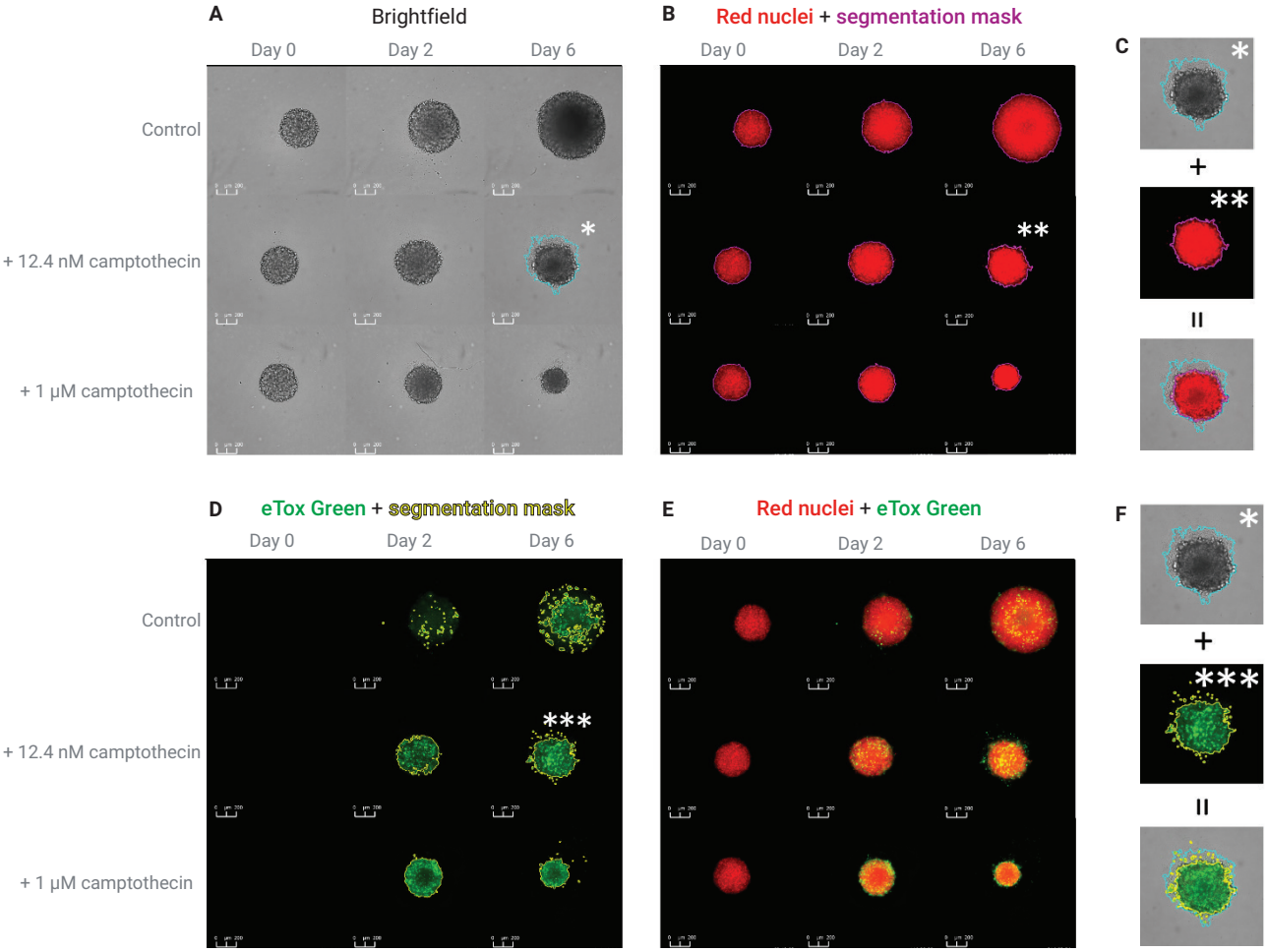


**Figure 4.** Select images showing the time- and dose-dependency of camptothecin-mediated shrinkage of HT-1080 Red spheroids. (A) Brightfield alone. The brightfield segmentation mask is shown in cyan for only one of the images (marked by an asterisk). (B) Red fluorescence (derived from nuclear-localized RFP) + corresponding segmentation mask (pink). Double asterisks highlight the same spheroid that has a single asterisk in panel A. (C) Superimposition of the brightfield image from panel A (marked with a single asterisk) with the red fluorescent image from panel B (marked with double asterisks). The cyan and pink outlines demarcate the boundary of the spheroid based on brightfield and red fluorescence, respectively. (D) Green fluorescent dead cell marker (eTox Green) and its corresponding segmentation mask (yellow). (E) Nuclear RFP-derived red fluorescence superimposed with the green eTox dead cell marker. (F) Superimposition of the brightfield image from panel A (marked by a single asterisk) with the green fluorescent dead cell image from panel D (marked with triple asterisks). The cyan and yellow outlines demarcate the boundary of the spheroid based on brightfield and green fluorescence, respectively. All scale bars = 200 µm.

carbocyanine dead cell dye). The existence of these anomalously stained regions should be considered when determining how to best analyze data.

Consistent with the brightfield challenges described above, attempting to quantify camptothecin efficacy using the brightfield area of spheroids yielded data of poor quality (not shown). In contrast, plotting either the red area (Figure 5A) or the red integrated intensity (Figure 5B) of the HT-1080 Red spheroids clearly demonstrates dose-dependent killing by camptothecin. Plotting the area under these curves versus the camptothecin concentration produced the dose-response curves in Figure 5C.

Importantly, the $IC_{50}$ values derived from analyzing spheroid red area versus spheroid red intensity are very similar (table insert in Figure 5C).

Plotting the intensity of the green dead cell dye as a function of time reveals the complex nature of this readout (Figure 5D). Even focusing the analysis on the first 50 hours, where the signal seems to display a clearer dependence on drug concentration, did not yield reasonable $IC_{50}$ values (not shown). This suggests that although dead cell stains such as eTox Green are helpful for identifying the location/distribution of dead cells within a spheroid, they may be less useful for the purpose of quantifying drug efficacy.

## Comparing drug efficacy in 2D versus 3D models

An important attribute of spheroids is their ability to mimic the drug resistance/sensitivity of solid tumors more faithfully than 2D monolayers. This is due to a variety of factors, including the differential gene expression profiles and growth rates of cells within 2D versus 3D microenvironments, the challenge of drugs penetrating to a spheroid's interior, etc. To probe how the sensitivity of HT-1080 Red cells varies as a function of assay format, these

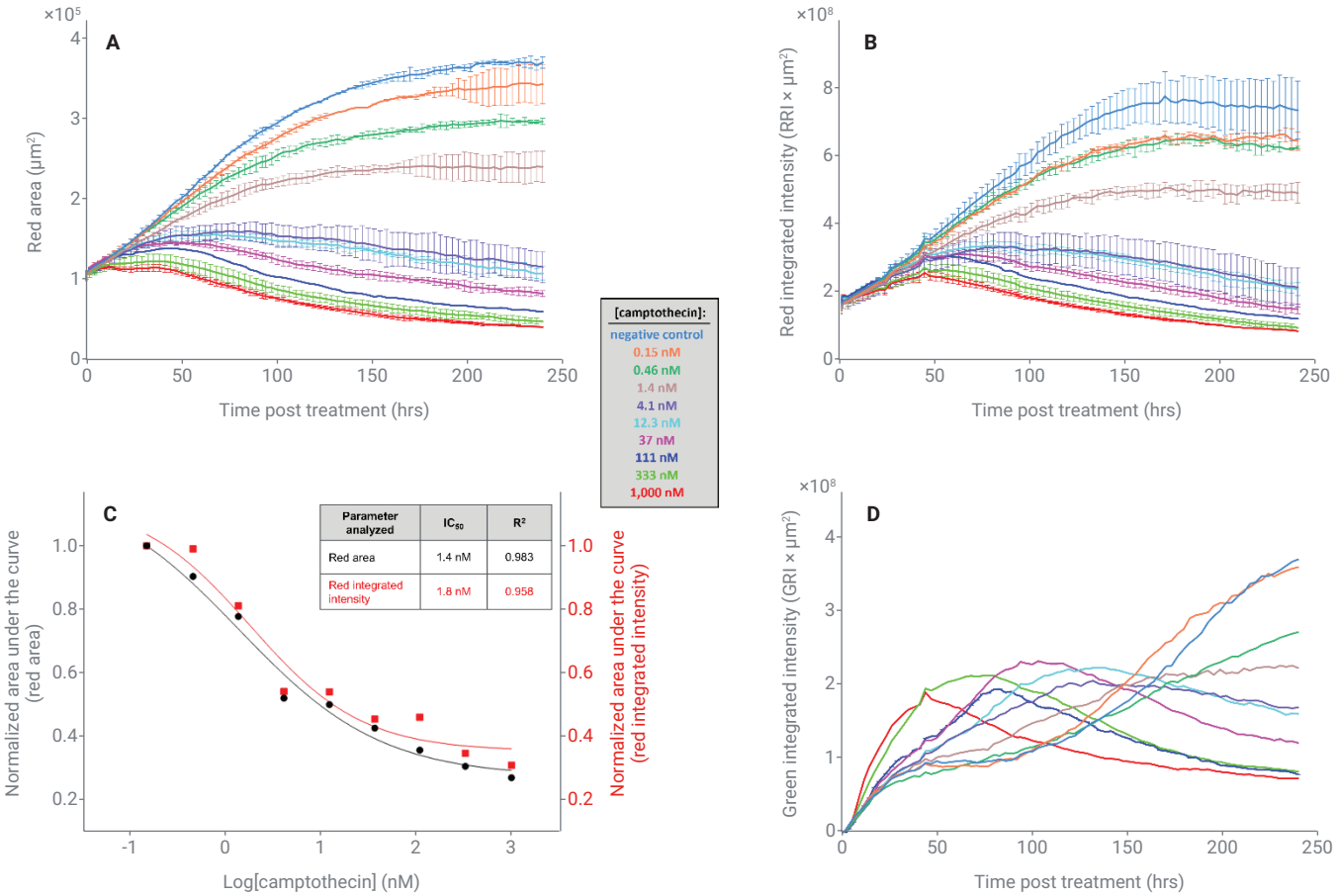


**Figure 5.** Characterizing camptothecin-mediated shrinkage of HT-1080 Red cells. (A) The red area of spheroids as a function of time. (B) The red integrated intensity of spheroids as a function of time. (C) Dose response curves produced by plotting the area under the curves (AUC) from panels A and B as a function of camptothecin concentration. So that both data sets could be plotted using similar Y-axis scales, AUC values were normalized using the following equation: Normalized AUC = ($AUC_{concentration\ of\ interest}$ /$AUC_{lowest\ concentration}$). (D) Green integrated intensity, reflecting cell death, as a function of time. Standard deviation error bars are removed to make it easier to see trends within the data traces.

cells were seeded into either electronic E-Plates (forming 2D monolayers) or round-bottom HLA plates (forming spheroids). Different concentrations of camptothecin were added to the 2D monolayer 24 hours after seeding, and cytotoxicity was subsequently monitored by counting the number of red cells over time. The same drug treatments were also added to the spheroids 3, 5, or 7 days after seeding, and cytotoxicity was monitored using red total area. Figures 6A and 6B clearly demonstrate that, relative to a 2D monolayer, the spheroids are more resistant to camptothecin. Importantly, the drug sensitivity of these spheroids is highly dependent on the time at which drug is added. This phenomenon has been described by others in the literature, and should be kept in mind when attempting to maximize the reproducibility of spheroid assays.

**A**

| Assay Format | $IC_{50}$ | $R^2$ |
|---|---|---|
| 2D | 0.79 nM | 0.9711 |
| 3D, Drug Added on Day 3 | 1.40 nM | 0.9825 |
| 3D, Drug Added on Day 5 | 6.20 nM | 0.9729 |
| 3D, Drug Added on Day 7 | 15 nM | 0.9868 |

**B**

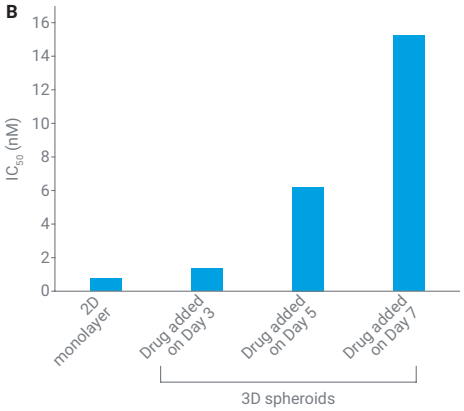


**Figure 6.** Evaluating the efficacy of camptothecin within different assay formats. Tabular (A) and graphical (B) representations of $IC_{50}$ values. See text for details.

## Quantifying assay robustness for high-throughput screening

Ideal drug screening assays differentiate "hits" from "nonhits" easily and with high confidence. This is accomplished when there is a large difference between the signal of hits versus nonhits, and when the standard deviation is small. One way to quantify the quality/efficacy/robustness (i.e. statistical effect size) of a screening assay is through the use of the Z'-factor, where:

$$Z' = 1 - \frac{3(\sigma_p + \sigma_n)}{|\mu_p - \mu_n|}$$

and μ and σ represent the mean and standard deviation of both the positive (p) and negative (n) controls. Using criteria defined in reference 7, Z'-factor scores less than zero indicate that there is too much overlap between negative and positive controls for the assay to be useful. While scores of 0 to 0.5 indicate that an assay is marginally useful, scores of 0.5 to 1 indicate that the assay is an excellent screening tool.

To determine the Z'-factor for the eSight 3D spheroid assay, HT-1080 Red spheroids were grown in a round-bottom HLA plate as described above. Three days after seeding cells, 48 wells were treated with 0.1% DMSO as the negative control, while the other 48 wells were treated with 1 μM camptothecin as the positive control. Three days after drug addition, spheroid diameters were quantified using either brightfield or red fluorescent images.

Showing only 12 wells for each of the conditions, Figure 7A demonstrates progressive growth of the negative control, shrinkage of the positive control, and a high degree of consistency in spheroid size for each condition. Whereas Z'-factor is typically calculated for a single time point, the continuous nature of the eSight assay makes it possible to evaluate Z'-factor over the entire time course. Figure 7B shows that immediately after drug addition the Z'-factor is quite low, but increases steadily. By roughly 25 hours post drug addition the Z'-factor surpasses a value of 0.5, and it eventually reaches its maximum value of ~0.8 around the 100 hour time point. The lag phase observed here is to be expected; it simply takes 25 hours for camptothecin's toxicity to manifest as a substantial change in spheroid size. This assessment of Z'-factor indicates that the eSight 3D spheroid assay can function as a robust screening tool, but it also helps define the optimal time window over which analyses should be conducted. Finally, Z'-factor calculations based on brightfield diameter are nearly identical to those based on red fluorescent diameter (Figure 7B). This contrasts with what was observed in Figures 4 and 5 where fluorescent images yielded higher quality data than brightfield images did. This seems to be a consequence of drug concentration, and is discussed further in the Conclusion section which follows.

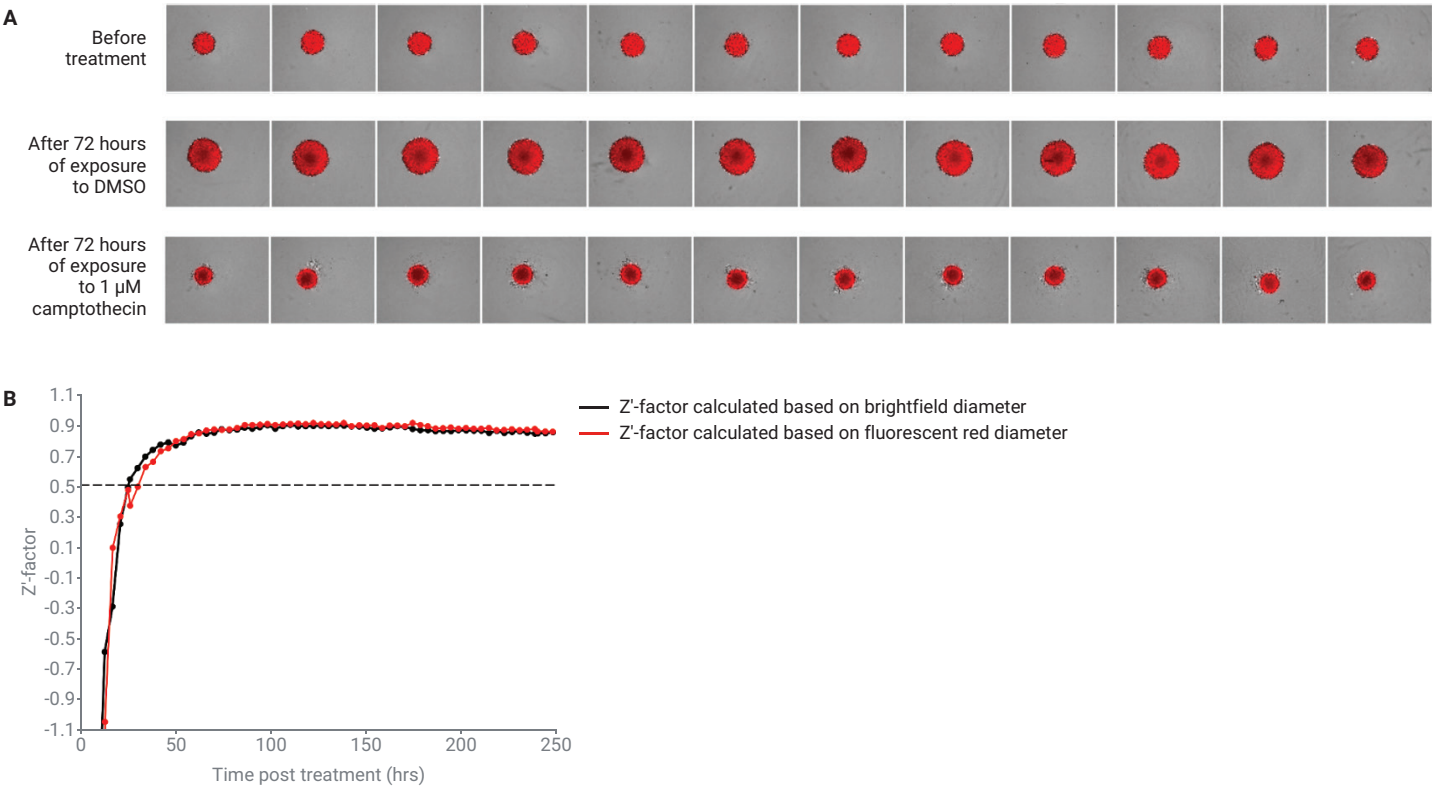


**Figure 7.** Using Z'-factor to evaluate the efficacy of the eSight 3D spheroid assay as a screening tool for anticancer drugs. (A) Images of HT-1080 Red spheroids immediately before treatment, and after 3 days of exposure to either the DMSO negative control or 1 µM camptothecin. Although many more wells were interrogated for each condition, only a row of 12 wells is shown for each condition. (B) Z'-factor as a function of time. Z'-factor was calculated using the diameter of spheroids based on either brightfield images or red fluorescent images. The horizontal dashed line at a value of 0.5 denotes the cutoff point above which an assay is considered to be highly effective for identifying drugs with the desired properties.

## Conclusion

The eSight 3D spheroid assay described in this application note enables spheroids to be generated easily and analyzed continuously over assay windows spanning many days. Beyond seeding cells, the only other hands-on step that is required is the addition of drug. For the purposes of initially identifying drug hits and subsequently quantifying the efficacy of these hits, eSight's software analyzes a variety of spheroid growth/shrinkage metrics. Since every cell type displays unique behaviors when grown in 3D, eSight's array of analysis tools should be tested and thoughtfully considered on a case-by-case basis.

For the HT-1080 Red cells used here, high concentrations of camptothecin cause spheroids to decrease in size while still maintaining a tight unambiguous perimeter. This appears to be due to efficient lysis of peripheral cells. In this context, spheroid size could be analyzed equally effectively using brightfield and fluorescent images (Figures 4 and 7). In contrast, intermediate camptothecin concentrations give rise to spheroids with loose ambiguous perimeters that are more difficult to analyze using brightfield alone. Note that these challenging structures can potentially result from dying cells that remain attached to the spheroid's periphery, as well as cells/debris that have sloughed off the spheroid and settled to the well bottom. The reason for the anomalous staining patterns in this peripheral material has not yet been explored. Compared to using brightfield alone, the use of endogenously expressed fluorescent proteins seems to be a more foolproof means of tracking spheroid viability. In instances where lentivirus-derived stable cell lines are not an option, cell nuclei can be labeled simply by including Agilent eLive Red/Green dyes in the spheroid growth medium.

Finally, it is worthwhile to discuss the use of intensity measurements in 3D assays. When operating in its 3D spheroid mode, eSight collects photos in multiple focal planes and then superimposes them to yield a single output photo. The "integrated intensity" of the spheroid as a whole is calculated simply by summing the total integrated intensity of all the focal planes. This approach does not exhaustively account for light emitted from the entire spheroid volume. However, because the exact same process is used across all wells of the plate, this is an efficient means of making relative comparisons between wells and tracking changes over time.

## References


1. Horvath, P. *et al.* Screening Out Irrelevant Cell-Based Models of Disease. *Review Nat. Rev. Drug Discov.* **2016**, *15(11)*, 751–769.
2. Kapałczyńska, M. *et al.* 2D and 3D Cell Cultures - a Comparison of Different Types of Cancer Cell Cultures. *Arch. Med. Sci.* **2018**, *14(4)*, 910–919.
3. Glimelius, B. *et al.* Extracellular Matrices In Multicellular Spheroids of Human Glioma Origin: Increased Incorporation of Proteoglycans and Fibronectin as Compared to Monolayer Cultures. *APMIS* **1988**, *96(5)*, 433–44.
4. Riffle, S. *et al.* Modeling Tumor Cell Adaptations to Hypoxia in Multicellular Tumor Spheroids. *J. Exp. Clin. Cancer Res.* **2017**, *36*, 102.
5. Groebe, K. *et al.* On the Relation Between Size of Necrosis and Diameter of Tumor Spheroids. Int. *J. Radiat. Oncol. Biol. Phys*. **1996**, *34(2)*, 395–401.
6. Millard, M. *et al.* Drug Delivery to Solid Tumors: the Predictive Value of the Multicellular Tumor Spheroid Model for Nanomedicine Screening. *Int. J. Nanomedicine* **2017**, *12*, 7993–8007.
7. Ji-Hu, Z. *et al.* A Simple Statistical Parameter for Use in Evaluation and Validation of High Throughput Screening Assays. *J. Biomol. Screen.* **1999**, *4(2)*, 67–73.


**www.agilent.com/chem/esight**




RA44610.7046064815





Printed in the USA, March 24, 2022
5994-4680EN